REVIEW

nature structural & molecular biology

Cryo-electron microscopy snapshots of the spliceosome: structural insights into a dynamic ribonucleoprotein machine

Sebastian M Fica & Kiyoshi Nagai

The spliceosome excises introns from pre-messenger RNAs using an RNA-based active site that is cradled by a dynamic protein scaffold. A recent revolution in cryo-electron microscopy (cryo-EM) has led to near-atomic-resolution structures of key spliceosome complexes that provide insight into the mechanism of activation, splice site positioning, catalysis, protein rearrangements and ATPase-mediated dynamics of the active site. The cryo-EM structures rationalize decades of observations from genetic and biochemical studies and provide a molecular framework for future functional studies.

During eukaryotic gene expression, genes are first transcribed into pre-messenger RNAs (pre-mRNAs), in which the coding information (represented by exons) is interrupted by introns. To produce mature messenger RNAs (mRNAs) with an uninterrupted protein coding sequence, introns are excised from pre-mRNAs by two sequential phosphoryl-transfer reactions—branching and exon ligation[1–4] (**Fig. 1a**). During branching the 2′ hydroxyl of a conserved adenosine, called the branch point (BP), attacks a phosphate at the 5′ splice site (5′-SS) to produce a free 5′ exon and a lariat intron–3′ exon intermediate, whereas during exon ligation the new 3′ hydroxyl group of the 5′ exon attacks a phosphate at the 3′ splice site (3′-SS) to ligate the exons and release the lariat intron. These reactions are chemically simple but catalyzed by a dynamic ribonucleoprotein enzyme, the spliceosome, which is comprised of five small nuclear RNAs (snRNAs) and over 70 proteins in yeast. The spliceosome is not a preformed enzyme, and the active site is created only after the spliceosome, which is assembled on pre-mRNA from many components, has undergone extensive conformational and compositional changes[5,6] (**Figs. 1b** and **2**). Because of its dynamic nature, understanding the molecular mechanism of splicing has been an enormous challenge for structural biologists.

The spliceosome assembles *de novo* on each intron of the pre-mRNA in a stepwise manner from individual small nuclear ribonucleoprotein particles (snRNPs) that are composed of snRNA and associated proteins[5,6]. Five snRNPs (U1, U2, U4, U5 and U6 snRNPs), named after their snRNA component, associate with a pre-mRNA (**Fig. 1b**). Several key RNA-recognition and remodeling events occur during activation, in addition to numerous changes in protein composition, to create the active site[5,6]. Four decades of biochemical and genetic studies have established a series of assembly and remodeling steps that underlie the precise functioning of this intricate molecular machine. The U1 and U2 snRNPs first pair with the 5′-SS and the BP of the pre-mRNA, respectively[7–10], which leads to formation of the A complex[11] (**Fig. 1b**). Assembly then proceeds with association of the U4/U6–U5 tri-snRNP[11] (**Figs. 1b** and **2**), in which the U6 snRNA is extensively base-paired with the U4 snRNA[12]. In the resulting pre-B complex, the U1 snRNP remains bound to the 5′-SS; however, the ATPase Prp28 promotes dissociation of the U1 snRNP[13] to form a stable B complex[14] (**Figs. 1b**, **2** and **3a**). To enable catalytic activation, the ATPase Brr2 dissociates the U4 snRNA[15,16], which allows the U6 snRNA to adopt a catalytically active structure together with the U2 snRNA[17] and to pair with the 5′ end of the intron[18,19] (**Figs. 3b** and **4**). Elucidation of base-pairing between the U6 and U2 snRNAs and the pre-mRNA revealed RNA elements that are structurally similar to those present in group II self-splicing introns[20,21], suggesting that their active sites might be structurally similar (**Fig. 4**). The B^{act} complex, which contains the U2, U5 and U6 snRNAs, forms after the B complex is remodeled by Brr2 and stabilized by a complex of proteins associated with Prp19 (termed the NTC), together with NTC-related factors[22–24] (**Figs. 2** and **5**). The ATPase Prp2 then promotes the binding of branching factors and juxtaposition of the 5′-SS and the BP for branching[25–27] (**Figs. 3** and **4**). The resulting B* complex catalyzes branching to form the C complex (**Figs. 2**, **3c** and **4e**). After the first catalytic reaction, the ATPase Prp16 remodels the spliceosome to allow dissociation of the branching factors[28,29] and enable docking of 3′-SS into the active site[27,30] with the help of exon ligation factors[31]. The 5′ and 3′ exons are aligned by the U5 snRNA[32,33], and the resulting spliceosomal C* complex performs the second catalytic step (**Figs. 1**, **2** and **4**). The ATPase Prp22 then releases the mRNA[34,35], and the ATPases Prp43 and Brr2 disassemble the spliceosome[36,37] (**Figs. 1** and **2**).

A cryo-EM revolution

Crystal structures of key protein components—such as Prp8 (refs. 38–42) and Brr2 (refs. 43–46), the Sm[47] and LSm[48] protein complexes, the Snu13–Prp31–U4 snRNA complex[49], the SF3a (ref. 50) and SF3b (ref. 51) complexes, and the functional core of the U1 snRNP[52–54]—have provided structural insights and complemented the functional

MRC Laboratory of Molecular Biology, Cambridge, UK. Correspondence should be addressed to S.M.F. (sfica@mrc-lmb.cam.ac.uk) or K.N. (kn@mrc-lmb.cam.ac.uk).

Received 20 June; accepted 10 August; published online 05 October 2017; doi:10.1038/nsmb.3463

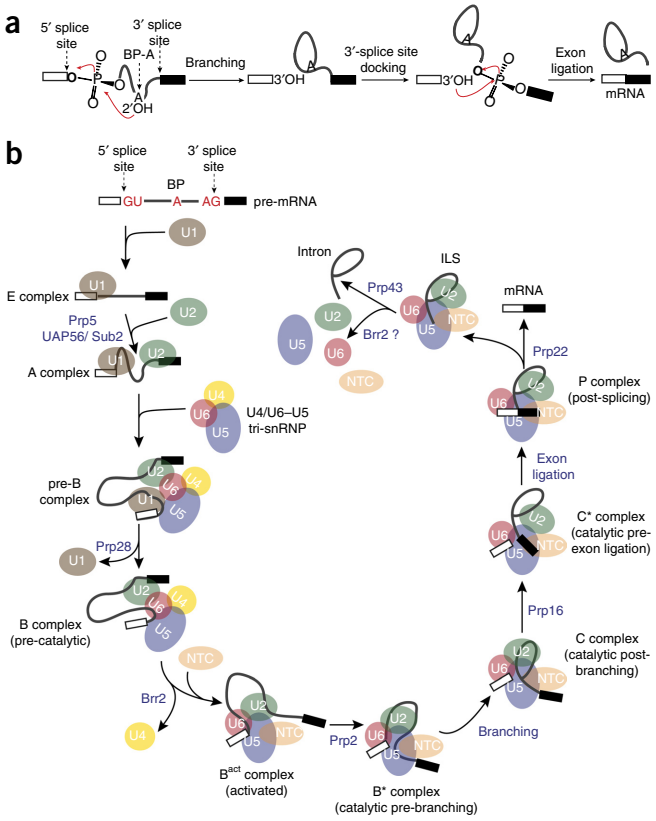

Figure 1 A functional view of the splicing cycle. (**a**) Two-step mechanism of pre-mRNA splicing. (**b**) Assembly and catalytic cycle of the spliceosome.

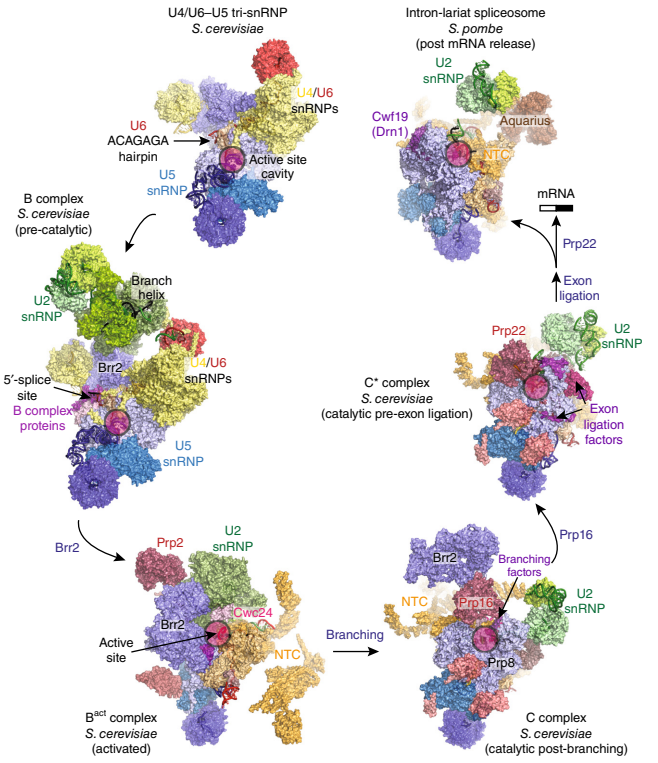

Figure 2 A structural view of the splicing cycle. Complexes for which high-resolution structures were solved by cryo-EM are shown in surface representation. Key features are indicated for each complex (for example, the location of the active site). Major subcomplexes are colored as follows: U5 snRNP in blue, U6 snRNP in red, U4 snRNP and U4/U6 proteins in yellow, U2 snRNP in green, NTC and NTC-associated factors in orange and trans-acting protein factors in magenta. The following PDB entries were used: 5GAN (U4/U6–U5 tri-snRNP); 5NRL (B complex); 5GM6 (Bact complex); 5LJ5 (C complex); 5MQ0 (C* complex); 3JB9 (ILS).

studies. However, an in-depth mechanistic understanding of spliceosome catalysis and dynamics requires high-resolution structures of fully assembled spliceosomes.

Previous negative-stain and cryo-EM studies of spliceosomes and spliceosomal snRNPs had revealed their overall shapes at low resolution and the location of some specific tagged components[55–61]. Recent advances in cryo-EM data acquisition and processing have ushered in a so-called 'resolution revolution' that has allowed structures of heterogeneous macromolecular assemblies to be determined to near-atomic resolution[62]. In the past two years three laboratories have applied the new EM methods to the structural study of the spliceosome. The outcome has been a series of near-atomic-resolution snapshots of fully assembled spliceosomes captured at key steps along the splicing pathway that are now allowing an unprecedented molecular view of the splicing cycle (**Fig. 2**).

Assembly and activation of the spliceosome

The U1 and U2 snRNPs recognize the 5′-SS[52,53] and BP of a pre-mRNA, leading to formation of the A complex, which associates with the U4/U6–U5 tri-snRNP to form the fully assembled pre-B complex[14] (**Fig. 1b**). Following Prp28-dependent U1 snRNP release and association of the B complex proteins, the pre-B complex is converted to the stable B complex[14] (**Figs. 1b**, **2**, **3a** and **5**), which subsequently undergoes an extensive rearrangement of the RNA components, as well as changes in protein composition[63], to become the catalytically activated Bact complex (**Figs. 2**, **4d** and **5**). The structures of the B (ref. 64) and Bact (refs. 65,66) complexes provide a first glimpse into the activation mechanism (**Fig. 5**). In the B complex, the U2/U6 helix II, which is formed between the 5′ end of the U2 snRNA and the 3′ end of the U6 snRNA, holds the U2 snRNP and tri-snRNP firmly together in addition to more flexible interactions between the protein components of U4/U6–U5 tri-snRNP and the U2-snRNP-bound pre-mRNA[64] (**Figs. 2** and **5**). The conserved UACUAAC sequence around the BP of the pre-mRNA pairs with the U2 snRNA to form the branch helix within the context of the U2 snRNP (**Figs. 3a** and **6a**). The HEAT repeats in Hsh155, a component of the SF3b complex, binds the branch helix (**Fig. 3a**). The active site of the N-terminal helicase cassette in Brr2 is bound to the single-stranded region of the U4 snRNA and is poised to translocate along U4 snRNA and unwind the U4/U6 snRNA duplex (**Fig. 5**). A U6 snRNA hairpin containing the ACAGAGA 5′-SS binding region, which is stabilized by Dib1 in the structure of free tri-snRNP (refs. 67–69), is further stabilized by B complex proteins and now weakly interacts with the 5′-SS (**Figs. 2** and **5**). This suggests that in yeast, in the absence of NTC proteins, Prp28 activity is not sufficient for stable U6 exchange at the 5′-SS, consistent with functional studies[13,23]. Nonetheless, B complex proteins stabilize this initial 5′ exon tethering and, through interactions with Brr2, may couple initial weak recognition of the 5′-SS to Brr2 activation and U4/U6 unwinding. Although it is still base-paired with U4, the U6 snRNA already forms the U2/U6 helix II in the B complex (**Fig. 5**), a structure that likely primes the U6 and U2 snRNAs to fold into the catalytically active RNA structure when the U6 snRNA is freed from the U4 snRNA by Brr2 action[64]. During this process at least 24 proteins (including the U4/U6–U5 tri-snRNP and the B complex

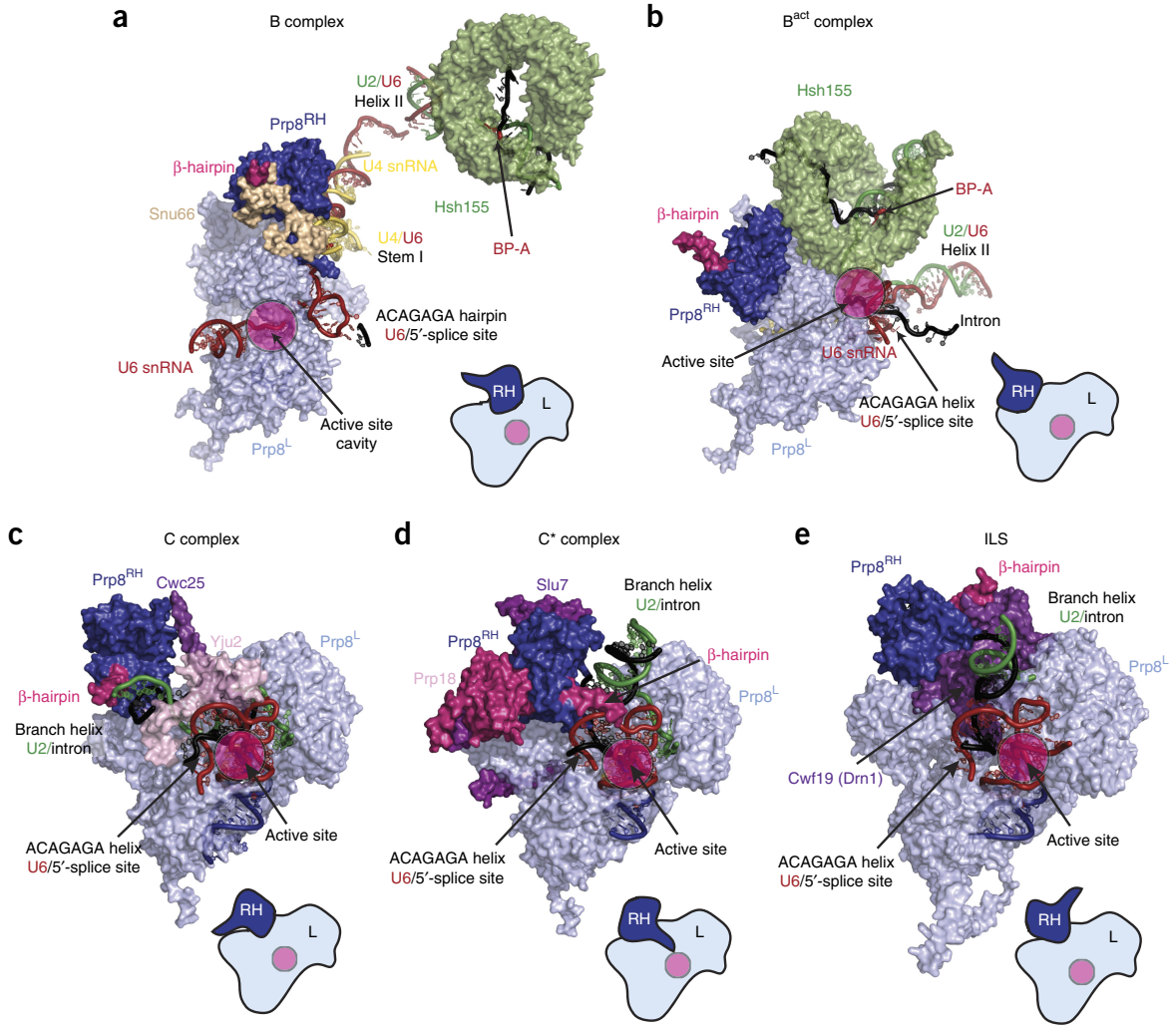

Figure 3 Movement of the Prp8 RNaseH-like domain and its interaction with active site elements. (**a**–**e**) Surface representation of the position and key interacting partners of the Prp8 RNaseH-like (Prp8^{RH}) domain in the B (**a**), B^{act} (**b**), C (**c**), C* (**d**) and ILS (**e**) spliceosomal complexes, relative to the Prp8 Large (Prp8^{L}) domain. The insets show the relative movement of the domain. The Prp8^{RH} domain rotates during the catalytic phase of splicing and mediates conformational changes in the active site.

proteins) dissociate from, and numerous NTC and NTR proteins join, the spliceosome[63] (**Figs. 2** and **5**).

The active site of the spliceosome, which is reminiscent of the group II intron active site[20,21], is fully formed during the transition of the B complex to the B^{act} complex, and it remains unchanged during the two phosphoryl-transfer reactions (**Fig. 4d**–**f**). The 5′-SS is correctly positioned in the active site owing to the pairing between the 5′ end of the intron and the U6 snRNA ACAGAGA sequence[18,19], as well as to the tethering of the 5′ exon to the U5 snRNA loop 1 (refs. 32,33) (**Fig. 4a**). The 5′ exon is further clamped together with Cwc21 between the N-terminal and linker domains of Prp8 when the U5 snRNP foot domain undergoes a rotation, which may be induced by the dissociation of B complex proteins and initial unwinding of the U6 ACAGAGA stem. The B^{act} complex is kept inactive by the U2 snRNP SF3b subcomplex, which encircles the BP and sequesters the branch helix more than 50 Å away from the catalytic Mg^{2+} ions[65,66] (**Figs. 3b**, **4d** and **5**). The overall architecture of the B^{act} complex is held together by the NTC (**Figs. 2** and **5**), whose components function as a multipronged clamp that restrains the many intricate RNA interactions that are crucial for catalysis. Indeed, specific NTC-associated factors, such as Cwc24, replace B complex proteins (**Fig. 2**) and seem to regulate recognition of the 5′-SS and its docking at the catalytic Mg^{2+} site; functional studies have further confirmed the importance of such factors in the stabilization of the B^{act} complex before Prp2 activity[70]. Together the B and B^{act} structures reveal key transitions of the snRNAs during formation of the active site, and they provide a molecular basis for understanding the role of the NTC and NTR proteins in spliceosome activation (**Fig. 5**).

The active site

Cryo-EM structures of the *Saccharomyces cerevisiae* C complex[71,72] have revealed the structure of the active site in a catalytically active spliceosome that is bound by the products of the first phosphoryl-transfer reaction (branching), a free 5′ exon and a lariat–3′ exon intermediate (**Figs. 2** and **4**). The U6 snRNA forms an intramolecular stem-loop (ISL) structure and helices Ia and Ib with the U2 snRNA, as first demonstrated by elegant genetic experiments[17]. This produces a highly twisted backbone of the bulged nucleotides of the ISL, which together with the backbone of the U6 catalytic triad (A59, G60 and C61) forms binding sites for two catalytic magnesium ions, as

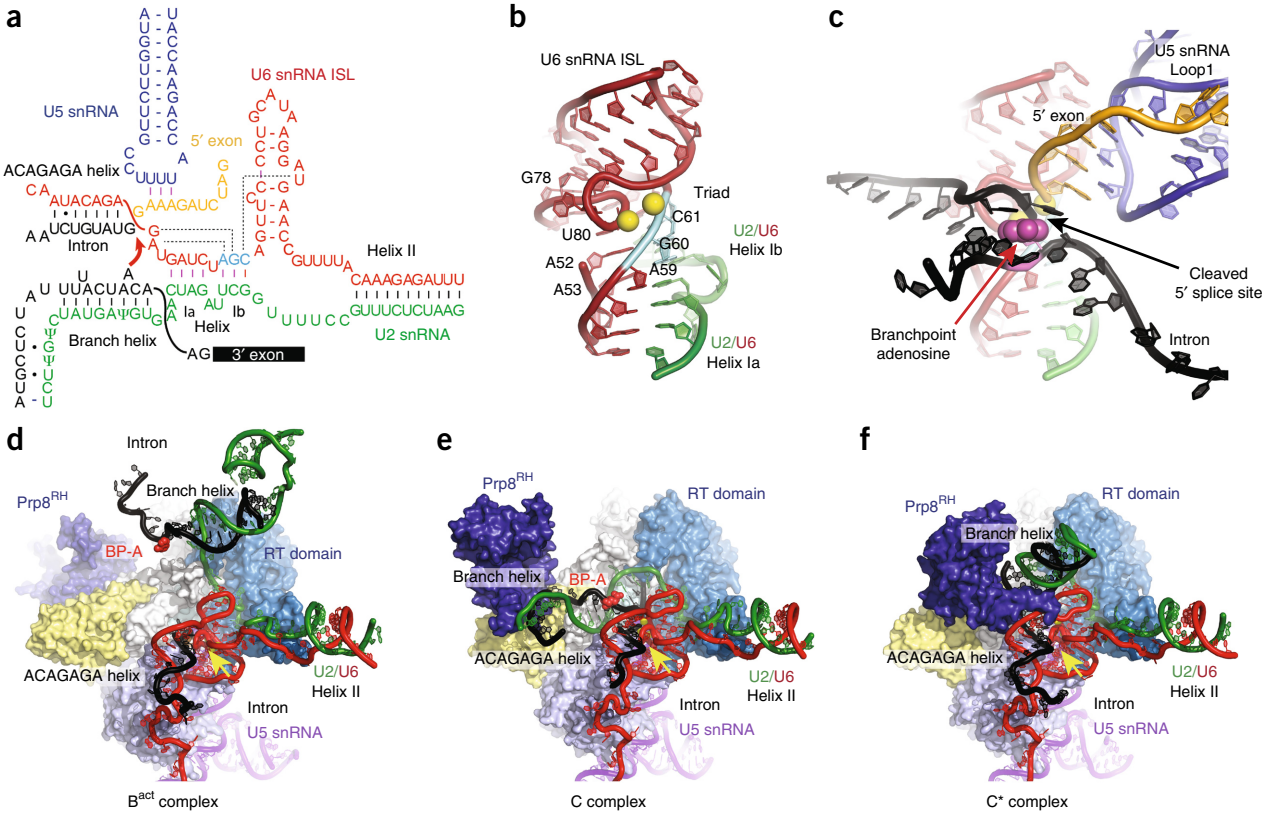

Figure 4 The active site of the spliceosome and its interaction with substrate. (**a**) The RNA interaction network before the first trans-esterification reaction. The U6 snRNA (red) forms an intramolecular stem-loop (ISL) and the helices Ia and Ib with the U2 snRNA. The three nucleotides that form the catalytic triad (AGC; in cyan) form three consecutive triple base-pairs with the U2 snRNA (green) nucleotides U80, U52 and U53 (the catalytic triplex). The first six nucleotides of the intron (black), GUAUGU, are base-paired with the ACAGAGA box in the U6 snRNA and interact with the branch helix[71,77]. The conserved UACUAAC (where A represents the BP adenosine) sequence in the intron base-pairs with the U2 snRNA to form the branch helix from which the BP adenosine bulges out. The hydroxyl group of this adenosine functions as a nucleophile that attacks the 5′-SS. The U5 snRNA is in blue, the 5′ exon is in orange, and the intron is in black. (**b**) Three-dimensional structure of the active site RNA in the C complex. Magnesium ions are represented by two yellow spheres located between the backbone of the catalytic triad and the highly twisted backbone at the bulge in the ISL. (**c**) structure of the 5′ exon and branched intron bound to the active site (overlaid on the structure in **b**). The base of the BP adenosine is shown as magenta spheres. The 5′ phosphate of the first intron nucleotide (G+1) forms a 2′-5′ phosphodiester bond with the 2′ hydroxyl of the BP adenosine. For clarity, the branch helix is not depicted. (**d**–**f**) Interaction of the catalytic core of the spliceosome and movement of the branch helix in the B^{act} (**d**), C (**e**) and C* (**f**) complexes. RNAs are color-coded as in **a**. The domains of Prp8 are color-coded[42] as follows: the N-terminal domain in light blue, the RT domain in aquamarine, the linker domain in white, the EN domain in light yellow, and the RH domain in deep blue. Note that the active site RNAs remain unchanged, but the branch helix shows large movements between the B^{act}, C and C* complexes. The branch helix is stabilized by SF3b (B^{act}), step 1 factors (C) and step 2 factors and the Prp8 RH domain (C*), respectively (see **Fig. 3**). The yellow arrows indicate the active site metals.

proposed by the two-metal ion mechanism[73] (**Fig. 4a**,**b**). Indeed, the catalytic Mg^{2+}-coordinating phosphate oxygens that were identified by metal-rescue experiments are in perfect agreement with the Mg^{2+} ligands observed in the structure[74,75]. The bases of A53, G52 and U80 form three consecutive triple base pairs[76] with U6/U2 helix Ib involving the catalytic triad (A59, G60 and C61), and the stacking of these triple base pairs (A53, G52 and U80) stabilizes the folded RNA structure, as observed in the active site of the group II intron[20,21] (**Fig. 4b**).

As a result of the branching reaction, the substrate pre-mRNA is cleaved at the 5′-SS, and the 5′ phosphate of the first intron nucleotide (G+1) forms a new 2′-5′ phosphodiester bond with the 2′ hydroxyl group of the BP adenosine to produce a lariat intron structure (**Figs. 1a** and **4c**). In the C complex, both the 3′ hydroxyl group of the 5′ exon and the 5′ phosphate of the first intron nucleotide remain close to the catalytic Mg^{2+} ions, suggesting that the configuration of the B* complex active site (before branching) can be restored readily with minimal structural changes. The 5′ exon is tethered by the conserved loop 1 of the U5 snRNA, as first demonstrated by genetic and cross-linking experiments[32,33]. The first six intron nucleotides (GUAUGU) are stringently conserved in yeast, and the Watson-Crick and non-Watson-Crick base pairs between this hexanucleotide and the U6 snRNA ACAGAGA box are able to position the 5′-SS in the active site[70,71] (**Fig. 4a**). In yeast the pre-mRNA sequence around the BP adenosine is conserved to be UACUAAC (where A denotes the BP adenosine), and this sequence pairs with the U2 snRNA to form the branch helix with the bulged BP adenosine[10]. The base of the BP adenosine (A70 in the *UBC4* pre-mRNA) is flipped out and interacts with the surrounding protein residues in the B and B^{act} complexes[63–65], whereas in the C complex it forms hydrogen bonds with the U68 base to create an unusual backbone structure that projects the 2′ hydroxyl group toward the 5′-SS. The branch helix in the C complex is significantly distorted from the canonical A form and is docked into the active site by the branching-specific proteins, Cwc25, Yju2 and Isy1 (**Figs. 2**, **3c** and **4e**) to insert the 2′ hydroxyl group of the BP adenosine into the active center.

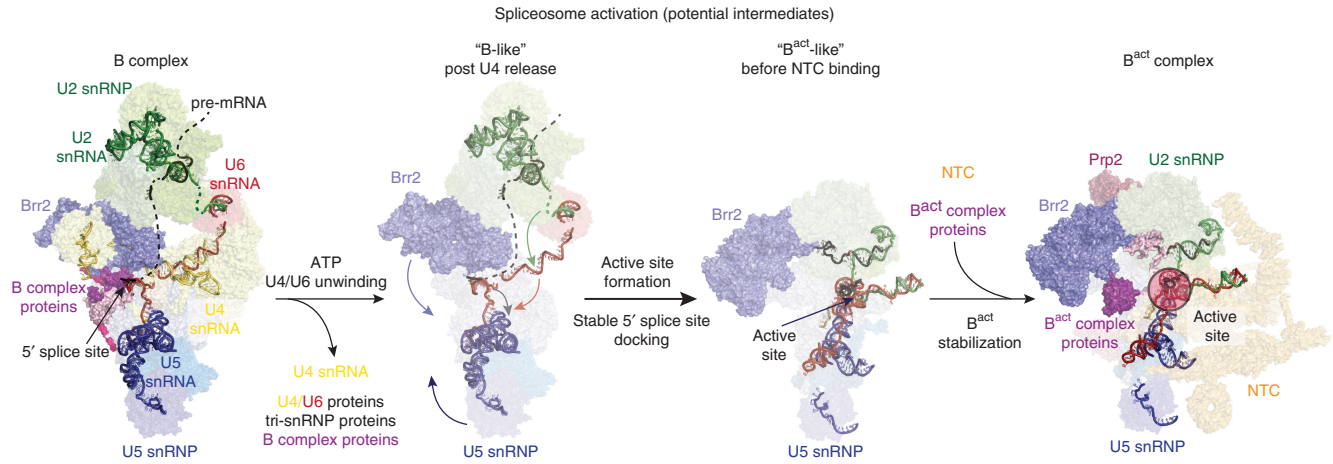

Figure 5 Activation of the spliceosome. A fully assembled spliceosome, the pre-B complex (not shown), is converted to a stable B complex after release of the U1 snRNP by the ATPase Prp28. Within the B complex, the single-stranded region of the U4 snRNA is already bound to the active site of the Brr2 helicase, which is ready to translocate along the U4 snRNA and free the U6 snRNA from the U4 snRNA and the U4/U6 di-snRNP proteins. In the resulting transition to the B^{act} complex, the U6 snRNA folds, pairs with the U2 snRNA and interacts with the NTC and NTR proteins. During this process, the U2, U5 and U6 snRNAs, together with the pre-mRNA substrate, form the catalytic RNA core, similar to that seen for the active site of group II introns (see **Fig. 4**).

The group II intron active site is stabilized by a network of RNA interactions with other RNA domains of the intron[20,21]. In the absence of such an RNA scaffold, the active site RNA of the spliceosome is stabilized by surrounding proteins (**Fig. 4d–f**). Prp8, the largest and most conserved protein in the spliceosome, forms four major domains connected by flexible linkers[42,68]: the N-terminal (N) domain; the 'Large' (L) domain that comprises the reverse transcriptase (RT), linker and endonuclease (EN) domains; the RNaseH-like (RH) domain; and the Jab1/MPN (Jab) domain. The RT domain is expanded by the helix bundle domain attached to its N terminus[42,68]. The U5 snRNA stems I and II are firmly bound to the N-terminal domain of Prp8 and secured by a Prp8 polypeptide that is fitted into the minor groove[64–69,71,72,77,78], while the exon-binding U5 snRNA loop 1 that is attached to stem I projects into the active site. The catalytic RNA core is accommodated in the active site cavity that is formed by the RT, EN and N domains[42] (**Fig. 4d–f**) and is clamped onto Prp8 by NTC and NTR proteins, such as Cwc2, Bud31, Ecm2, Cef1 and Clf1 and Syf2 (refs. 71,72) (**Fig. 3c**). These proteins act as a cradle for the active site RNA and remain bound throughout the catalytic phase of the spliceosome; hence, the structure of the RNA active site changes little between the B^{act} and C* complexes[65,66,71,72,77,78] (**Fig. 4d–f**). In contrast, the branch helix moves substantially during the catalytic stage. In the C complex the branch helix in docked into the active site by the branching-specific factors (Cwc25, Yju2 and Isy1)[71,72] (**Figs. 3c** and **4e**); after Prp16-induced release of these proteins, the branch helix is free to move and change its orientation between the two catalytic steps.

Remodeling for exon ligation

Cross-linking studies showed that the 5′ and 3′ exons are aligned by U5 snRNA loop 1 during exon ligation to allow the 3′ hydroxyl group of the 5′ exon to attack the 3′-SS[32,33]. The structure of the stalled C complex provides the first structural insights into the remodeling of the active site that is induced by the action of spliceosomal DEAH-box ATPases[71] (**Fig. 6**). Prp16 is poised to bind and translocate the intron downstream of the branch helix to destabilize branching-specific factors[71] (**Figs. 2** and **6b**). In the C complex, the 5′ exon is tethered by loop 1 of the U5 snRNA, and the terminal 3′ hydroxyl group of the 5′ exon is already positioned near the catalytic Mg^{2+} ions. However, the branch helix that is docked into the active site by branch-specific factors prevents access of an incoming 3′ exon to the active site (**Figs. 3c** and **4c**,**e**). This indicates that the active site of the spliceosome has to be remodeled to create space for binding of the 3′ exon. The structure of a C* spliceosome that was stalled right after Prp16 action but before exon ligation further elucidated the consequences of Prp16 action[77,78] (**Figs. 3c** and **6b**). As in the C complex, the catalytic RNA core is fastened onto Prp8 in the C* complex (**Figs. 1c**, **2** and **3d**) by proteins common to both steps, while the branch helix is rotated by ~75° as compared to its position in the C complex and is held in a new position by the Prp8 RH ($Prp8^{RH}$) domain and by Slu7 and Prp18 together with the repositioned Prp17 WD40 domain (**Figs. 3d**, **4f** and **6c**). A β-hairpin that protrudes from the $Prp8^{RH}$ domain is likely to play an important functional role, as several mutations that affect the first and second steps of splicing have been mapped to it[41]. The $Prp8^{RH}$ domain has rotated by ~80° and extends its β-hairpin through the minor groove of the branch helix toward Cef1 (**Figs. 3d**, **4f** and **6c**). The Prp17 WD40 domain binds across the β-finger of the $Prp8^{RH}$ domain and Cef1, which stabilizes the rotated $Prp8^{RH}$ domain (**Figs. 3d** and **4f**). Slu7 is essential for exon ligation but is dispensable when the distance between the BP and 3′-SS is shorter than nine nucleotides[77,79]. Although Slu7 stabilizes the reoriented $Prp8^{RH}$ domain, the precise role of Slu7 in promoting 3′ exon docking remains unclear. The rotation of the branch helix moves the BP adenosine out of the active site, together with the attached 5′ end of the intron linked to the BP adenosine, which creates a space for 3′-exon docking and reorganizes the pairing between the 5′-SS and the U6 ACAGAGA region[77,78] (**Fig. 4a**,**f**).

Structural basis for remodeling by DEAH-box ATPases

It has been proposed that, during the catalytic stage, the spliceosome exists in a dynamic equilibrium between several conformations[80] and that this equilibrium is modulated both by the action of trans-acting factors such as Prp2, Prp16 and Prp22 and by co-functioning step-specific factors[80–83] (**Figs. 3** and **6**). The cryo-EM structures of the B, B^{act}, C and C* complexes have visualized these conformational changes, including the dramatic movement of the $Prp8^{RH}$ domain, Prp17, Syf1 and Clf1, as well as the more subtle movement of the $Prp8^{EN}$ domain (**Figs. 2**, **3d** and **4f**). To modulate such transitions

throughout the catalytic stage, DEAH-box ATPases bind the intron at a similar position 3′ of the BP (or the ligated exon junction for Prp22) and induce movement of the branch helix, as well as of these proteins (**Fig. 6**), underscoring a common remodeling mechanism, as discussed below. These trans-acting ATPases have also been implicated in proofreading correct transitions through the pathway[84–86]. Biochemical studies suggested that DEAH-box ATPases, such as Prp16 and Prp22, act at a distance through a 'winching' mechanism that involves translocation toward, but not necessarily through, their remodeling targets[27].

In the B^{act} complex, Prp2 binds the intron downstream of the branch helix that is held by Hsh155 within the SF3b complex[65,66] (**Figs. 3b** and **6a**). Thus, translocation of Prp2 toward the BP could dissociate SF3a and SF3b from the intron, allowing the branch helix to dock into the active site[87]. In the C complex, Prp16 binds Prp8 in proximity to Cwc25 and is poised to bind the intron 3′ of the BP[71] (**Figs. 3c** and **6b**). Translocation toward the BP would destabilize Cwc25 from the $Prp8^{RH}$ domain, thus allowing binding of Slu7 and Prp18 to the $Prp8^{RH}$ domain[77]. Notably, this model for action at a distance implies that transient destabilization of the branch helix, and thus both Prp16- and Prp2-mediated remodeling, would depend on the stability of the branch helix, consistent with proofreading by both Prp2 and Prp16 for usage of the correct BP[83,85]. More broadly, the large movement of the branch helix from the B^{act} to the C and C* complexes (**Fig. 4d–f**) that is promoted by Prp2 and Prp16, respectively, could affect the stability of the RNA active site[76,88], enabling Prp2 and Prp16 to proofread the integrity of the active site. Indeed, Prp16 proofreads catalytic interactions between the U6 snRNA and the catalytic Mg^{2+} (refs. 77,89).

Notably, the cryo-EM structures revealed both 'open' and 'closed' conformations for the DEAH-box ATPases (**Fig. 6d**). Because the open conformation observed for Prp22 allows RNA binding, toggling between the open and closed states could underlie the mechanism of RNA translocation upon ATP hydrolysis (**Fig. 6d**).

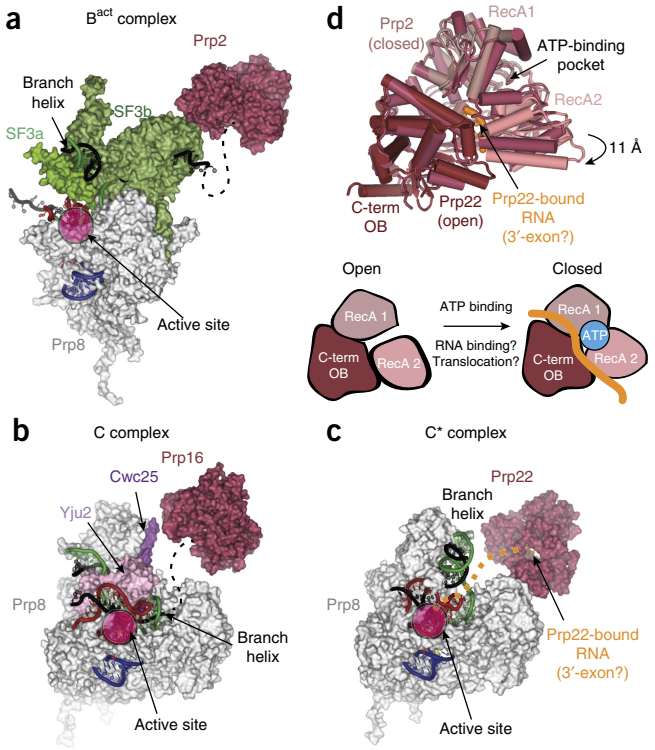

Figure 6 Binding of DEAH-box ATPases to specific spliceosomal complexes. (**a**–**c**) Surface representation of the positions and key interacting partners of DEAH-box ATPases, relative to Prp8, in the B^{act} (**a**), C (**b**) and C* (**c**) spliceosomal complexes. Key RNA components are shown in cartoon representations. The likely paths of the intron 3′ of the BP in B^{act} and C, and of the 3′ exon in C*, are indicated as dashed lines. (**d**) Top, different conformations of Prp2 and Prp22 observed in the cryo-EM maps of the B^{act} and C* complexes. Note that for Prp2 no bound RNA was modeled, and the RecA1 and RecA2 cassettes are present in a closed conformation, whereas for Prp22, bound RNA could be observed, and the RecA cassettes are present in an open conformation due to a downward movement of the RecA2 domain relative to the RecA1 domain. Bottom, the open and closed conformations are shown schematically in the lower diagram, in which the bound RNA is colored in orange. RecA1 and RecA2, RecA homology domains; C-term OB, C-terminal oligonucleotide-binding domain.

Dynamics of the $Prp8^{RH}$ domain

The structure of the $Prp8^{RH}$ domain was one of the first domain structures of Prp8 to be determined, and it attracted much attention[39–41]. On the basis of cross-linking and genetic experiments it was proposed that the $Prp8^{RH}$ domain might be part of the spliceosome active site[90–92]. The cryo-EM structures of the B^{act}, C and C* complexes now show that this is not the case. In the crystal structure of Prp8, the linker between the preceding $Prp8^{L}$ domain and the $Prp8^{RH}$ domain was disordered, suggesting that the $Prp8^{RH}$ domain could change its position with respect to the $Prp8^{L}$ domain during the splicing cycle[42]. Cryo-EM structures have now revealed that the $Prp8^{RH}$ domain moves significantly during the splicing cycle (**Fig. 3**). Dissociation of SF3b induced by Prp2 allows rotation of the branch helix and docking at the active site[65,66,71,72,87] (**Figs. 2**, **3b** and **4f**), whereas dissociation of Cwc24 and Cwc27 permits binding of Cwc25, Yju2 and Isy1 to clamp the branch helix in the conformation necessary for branching[71,72] (**Figs. 3c**, **4e** and **6a**). In this C conformation, the $Prp8^{RH}$ domain moves into the body of the complex, while the β-hairpin binds along the extended branch helix and stabilizes its position in cooperation with Yju2 (**Figs. 3c** and **4e**). The N terminus of Cwc25 interacts with the $Prp8^{RH}$ domain, and together they triangulate interactions that lock the branch helix in its first-step conformation. Notably, the $Prp8^{RH}$ domain together with the NTC factor Syf1 holds the 3′ domain of the U2 snRNP. Thus, the $Prp8^{RH}$ domain has now moved closer to the active site and could impact the conformation of the branch helix. Indeed, following Prp16 action, the branch helix in the C* complex undergoes a dramatic conformational change to form an extended helix that is rotated ~75° from its position in the C complex[77] (**Figs. 3d** and **4f**). This is accompanied by an 80° inward rotation of the $Prp8^{RH}$ domain. The β-hairpin now extends in the minor groove of the branch helix, contacts Cef1 and straddles the interface between the branch helix and the ACAGAGA helix, placing it proximal to the active site (**Fig. 3d**), although it is not directly part of the active site. Here the β-hairpin stabilizes the reorganized interaction between the 5′-SS and the U6 snRNA ACAGAGA sequence, particularly the new base pair between U(+2) of the intron and A51 in the U6 snRNA, which forms in C*. Indeed the β-hairpin interacts genetically with mutations at both U(+2) and A51 in U6 (refs. 91,92). The exon ligation factors Slu7 and Prp18 bind on the surface of the $Prp8^{RH}$ domain and lock it in the exon-ligation conformation, thus contributing to stabilization of the rotated branch helix.

Finally, in the post-splicing intron-lariat spliceosome (ILS) from *Schizosaccharomyces pombe*[93], the $Prp8^{RH}$ domain is rotated outward from the branch helix (**Fig. 3e**). The disassembly factor Cwf19 (Drn1 in yeast), which is important for recruitment of the debranching enzyme Dbr1 to the spliceosome[94], wedges between the $Prp8^{RH}$

domain and the branch helix. These conformational changes are likely the result of mRNA release following Prp22 activity. Overall the structures of specific spliceosomal complexes reveal that while remodeling the complex, the ATPases Prp2, Prp16 and Prp22 each cause dramatic movements of the Prp8^{RH} domain. The Prp8^{RH} domain stabilizes and modulates the conformation of the branch helix during the catalytic stage, with its β-hairpin likely affecting the Prp16-mediated transition between the C and C* complexes (**Figs. 3** and **6**).

Human spliceosome

The mechanism of splicing is likely to be universal; however, some details between yeast and human splicing may differ, particularly with regard to splice site selection. The sequences of the 5′-SS and BP are stringently conserved in yeast, whereas in humans they are much more degenerate. The 3′-SS and the polypyrimidine tract that precedes the 3′-SS in human introns are interrogated more than once during the splicing cycle, and the human spliceosome tolerates more sequence variability[6]. The structures of the human C* complex[95,96] provided a first glimpse of the human spliceosome and revealed the association of the exon junction complex (EJC) through the binding of Cwc22, which is deposited by the spliceosome approximately between −20 and −25 nucleotides upstream of the exon-exon junction and removed by the ribosome during translation. Positioning of the EJC in the structure is in good agreement with models based on the yeast C complex[71] and consistent with biochemical evidence[95]. It is notable that the human RBM22 protein shares homology with both yeast Cwc2 and Ecm2, even though the human spliceosome lacks individual homologs of yeast Cwc2 and Ecm2 (ref. 71). Additionally, mammal-specific exon ligation factors such as PRKRIP1 stabilize the C* complex and may impact the active site, whereas the NTC-related factor RBM22 probably cooperates with the ATPase Aquarius[97] to guide the intron toward the active site.

Structurally, free human U4/U6–U5 tri-snRNP differs significantly from its yeast counterpart. SAD1, a protein that associates with human tri-snRNP, keeps the BRR2 helicase away from its substrate U4 snRNA, whereas PRP28 is found in the open conformation near the N and Large domains of PRP8 (ref. 98). The pre-B complex that forms when the U4/U6–U5 tri-snRNP associates with the A complex is remodeled by PRP28, which dissociates U1 snRNP from the 5′-SS to form a stable B complex. A previous low-resolution EM reconstruction showed that the structure of the U4/U6–U5 tri-snRNP in the human B complex is similar to that of its yeast counterpart[99]. Now cryo-EM analysis has revealed that the structure of human B complex is remarkably similar to that of yeast B complex[100], except that the ACAGAGA helix is already formed in human B complex. Indeed, BRR2 helicase moves to a position found in the yeast tri-snRNP, in which the substrate U4 snRNA is bound in the active site of the BRR2 N-terminal helicase cassette[100], suggesting a conserved mechanism of pre-catalytic spliceosome assembly and activation.

Conclusions

The recent cryo-EM snapshots of the spliceosome allow a nearly complete structural view of key intermediates in the splicing pathway and provide an atomic framework to rationalize genetic and biochemical research from the last four decades. The structures reveal how this intricate molecular machine uses a single RNA-based active site to catalyze the branching and exon ligation reactions that excise introns from pre-mRNA. The structural snapshots visualize for the first time how the substrates and products of these two reactions are progressively docked and undocked at the active site using the ATP-powered actions of RNA helicases and how movement of specific domains in Prp8 promotes conformational toggling of the spliceosome.

Our challenge now is to use structural information to design further experiments to uncover the detailed inner workings and energetics of this dynamic machine, which will keep us busy for many years to come.

ACKNOWLEDGMENTS

We thank A. Newman, C. Plaschka, C. Charenton, L. Strittmatter and W. Galej for discussions and critical reading of the manuscript and C. Plaschka for drawing **Figure 5**. This work was funded by the UK Medical Research Council (grant no. MC_U105184330) and a European Research Council Advanced Grant (grant no. 693087–SPLICE3D). S.M.F. has been supported by EMBO and Marie Skłodowska-Curie fellowships.

COMPETING FINANCIAL INTERESTS

The authors declare no competing financial interests.

1. Padgett, R.A., Konarska, M.M., Grabowski, P.J., Hardy, S.F. & Sharp, P.A. Lariat RNAs as intermediates and products in the splicing of messenger RNA precursors. *Science* **225**, 898–903 (1984).
2. Domdey, H. *et al.* Lariat structures are *in vivo* intermediates in yeast pre-mRNA splicing. *Cell* **39**, 611–621 (1984).
3. Ruskin, B., Krainer, A.R., Maniatis, T. & Green, M.R. Excision of an intact intron as a novel lariat structure during pre-mRNA splicing *in vitro*. *Cell* **38**, 317–331 (1984).
4. Rodriguez, J.R., Pikielny, C.W. & Rosbash, M. *In vivo* characterization of yeast mRNA processing intermediates. *Cell* **39**, 603–610 (1984).
5. Staley, J.P. & Guthrie, C. Mechanical devices of the spliceosome: motors, clocks, springs and things. *Cell* **92**, 315–326 (1998).
6. Wahl, M.C., Will, C.L. & Lührmann, R. The spliceosome: design principles of a dynamic RNP machine. *Cell* **136**, 701–718 (2009).
7. Séraphin, B., Kretzner, L. & Rosbash, M. A U1 snRNA:pre-mRNA base-pairing interaction is required early in yeast spliceosome assembly but does not uniquely define the 5′ cleavage site. *EMBO J.* **7**, 2533–2538 (1988).
8. Zhuang, Y. & Weiner, A.M. A compensatory base change in U1 snRNA suppresses a 5′ splice site mutation. *Cell* **46**, 827–835 (1986).
9. Siliciano, P.G. & Guthrie, C. 5′ splice site selection in yeast: genetic alterations in base pairing with U1 reveal additional requirements. *Genes Dev.* **2**, 1258–1267 (1988).
10. Parker, R., Siliciano, P.G. & Guthrie, C. Recognition of the TACTAAC box during mRNA splicing in yeast involves base pairing to the U2-like snRNA. *Cell* **49**, 229–239 (1987).
11. Konarska, M.M. & Sharp, P.A. Interactions between small nuclear ribonucleoprotein particles in formation of spliceosomes. *Cell* **49**, 763–774 (1987).
12. Brow, D.A. & Guthrie, C. Spliceosomal RNA U6 is remarkably conserved from yeast to mammals. *Nature* **334**, 213–218 (1988).
13. Staley, J.P. & Guthrie, C. An RNA switch at the 5′ splice site requires ATP and the DEAD-box protein Prp28p. *Mol. Cell* **3**, 55–64 (1999).
14. Boesler, C. *et al.* A spliceosome intermediate with loosely associated tri-snRNP accumulates in the absence of Prp28 ATPase activity. *Nat. Commun.* **7**, 11997 (2016).
15. Laggerbauer, B., Achsel, T. & Lührmann, R. The human U5-200 kDa DEXH-box protein unwinds U4–U6 RNA duplices *in vitro*. *Proc. Natl. Acad. Sci. USA* **95**, 4188–4192 (1998).
16. Raghunathan, P.L. & Guthrie, C. RNA unwinding in U4/U6 snRNPs requires ATP hydrolysis and the DEIH-box splicing factor Brr2. *Curr. Biol.* **8**, 847–855 (1998).
17. Madhani, H.D. & Guthrie, C. A novel base-pairing interaction between U2 and U6 snRNAs suggests a mechanism for the catalytic activation of the spliceosome. *Cell* **71**, 803–817 (1992).
18. Lesser, C.F. & Guthrie, C. Mutations in U6 snRNA that alter splice site specificity: implications for the active site. *Science* **262**, 1982–1988 (1993).
19. Kandels-Lewis, S. & Séraphin, B. Involvement of U6 snRNA in 5′ splice site selection. *Science* **262**, 2035–2039 (1993).
20. Toor, N., Keating, K.S., Taylor, S.D. & Pyle, A.M. Crystal structure of a self-spliced group II intron. *Science* **320**, 77–82 (2008).
21. Robart, A.R., Chan, R.T., Peters, J.K., Rajashankar, K.R. & Toor, N. Crystal structure of a eukaryotic group II intron lariat. *Nature* **514**, 193–197 (2014).
22. Chan, S.-P., Kao, D.-I., Tsai, W.-Y. & Cheng, S.-C. The Prp19p-associated complex in spliceosome activation. *Science* **302**, 279–282 (2003).
23. Chan, S.-P. & Cheng, S.-C. The Prp19-associated complex is required for specifying interactions of U5 and U6 with pre-mRNA during spliceosome activation. *J. Biol. Chem.* **280**, 31190–31199 (2005).
24. Ohi, M.D. & Gould, K.L. Characterization of interactions among the Cef1p–Prp19p-associated splicing complex. *RNA* **8**, 798–815 (2002).
25. Chiu, Y.-F. *et al.* Cwc25 is a novel splicing factor required after Prp2 and Yju2 to facilitate the first catalytic reaction. *Mol. Cell. Biol.* **29**, 5671–5678 (2009).

26. Krishnan, R. *et al.* Biased Brownian ratcheting leads to pre-mRNA remodeling and capture prior to first-step splicing. *Nat. Struct. Mol. Biol.* **20**, 1450–1457 (2013).
27. Semlow, D.R., Blanco, M.R., Walter, N.G. & Staley, J.P. Spliceosomal DEAH-box ATPases remodel pre-mRNA to activate alternative splice sites. *Cell* **164**, 985–998 (2016).
This biochemical study proposed that DEAH-box ATPases bind away from their spliceosomal target and pull on the intron at a distance to remodel the spliceosome.
28. Tseng, C.-K., Liu, H.-L. & Cheng, S.-C. DEAH-box ATPase Prp16 has dual roles in remodeling of the spliceosome in catalytic steps. *RNA* **17**, 145–154 (2011).
29. Warkocki, Z. *et al.* Reconstitution of both steps of *Saccharomyces cerevisiae* splicing with purified spliceosomal components. *Nat. Struct. Mol. Biol.* **16**, 1237–1243 (2009).
30. Schwer, B. & Guthrie, C. A conformational rearrangement in the spliceosome is dependent on PRP16 and ATP hydrolysis. *EMBO J.* **11**, 5033–5039 (1992).
31. James, S.-A., Turner, W. & Schwer, B. How Slu7 and Prp18 cooperate in the second step of yeast pre-mRNA splicing. *RNA* **8**, 1068–1077 (2002).
32. Newman, A.J. & Norman, C. U5 snRNA interacts with exon sequences at 5′ and 3′ splice sites. *Cell* **68**, 743–754 (1992).
33. Sontheimer, E.J. & Steitz, J.A. The U5 and U6 small nuclear RNAs as active site components of the spliceosome. *Science* **262**, 1989–1996 (1993).
34. Company, M., Arenas, J. & Abelson, J. Requirement of the RNA-helicase-like protein PRP22 for release of messenger RNA from spliceosomes. *Nature* **349**, 487–493 (1991).
35. Schwer, B. A conformational rearrangement in the spliceosome sets the stage for Prp22-dependent mRNA release. *Mol. Cell* **30**, 743–754 (2008).
36. Tsai, R.T. *et al.* Spliceosome disassembly catalyzed by Prp43 and its associated components Ntr1 and Ntr2. *Genes Dev.* **19**, 2991–3003 (2005).
37. Fourmann, J.-B. *et al.* Dissection of the factor requirements for spliceosome disassembly and the elucidation of its dissociation products using a purified splicing system. *Genes Dev.* **27**, 413–428 (2013).
38. Pena, V., Liu, S., Bujnicki, J.M., Lührmann, R. & Wahl, M.C. Structure of a multipartite protein-protein interaction domain in splicing factor Prp8 and its link to retinitis pigmentosa. *Mol. Cell* **25**, 615–624 (2007).
39. Ritchie, D.B. *et al.* Structural elucidation of a PRP8 core domain from the heart of the spliceosome. *Nat. Struct. Mol. Biol.* **15**, 1199–1205 (2008).
40. Pena, V., Rozov, A., Fabrizio, P., Lührmann, R. & Wahl, M.C. Structure and function of an RNaseH domain at the heart of the spliceosome. *EMBO J.* **27**, 2929–2940 (2008).
41. Yang, K., Zhang, L., Xu, T., Heroux, A. & Zhao, R. Crystal structure of the β-finger domain of Prp8 reveals analogy to ribosomal proteins. *Proc. Natl. Acad. Sci. USA* **105**, 13817–13822 (2008).
42. Galej, W.P., Oubridge, C., Newman, A.J. & Nagai, K. Crystal structure of Prp8 reveals active site cavity of the spliceosome. *Nature* **493**, 638–643 (2013).
43. Santos, K.F. *et al.* Structural basis for functional cooperation between tandem helicase cassettes in Brr2-mediated remodeling of the spliceosome. *Proc. Natl. Acad. Sci. USA* **109**, 17418–17423 (2012).
44. Mozaffari-Jovin, S. *et al.* Inhibition of RNA helicase Brr2 by the C-terminal tail of the spliceosomal protein Prp8. *Science* **341**, 80–84 (2013).
45. Nguyen, T.H.D. *et al.* Structural basis of Brr2–Prp8 interactions and implications for U5 snRNP biogenesis and the spliceosome active site. *Structure* **21**, 910–919 (2013).
46. Pena, V. *et al.* Common design principles in the spliceosomal RNA helicase Brr2 and in the Hel308 DNA helicase. *Mol. Cell* **35**, 454–466 (2009).
47. Leung, A.K.W., Nagai, K. & Li, J. Structure of the spliceosomal U4 snRNP core domain and its implication for snRNP biogenesis. *Nature* **473**, 536–539 (2011).
48. Zhou, L. *et al.* Crystal structures of the Lsm complex bound to the 3′ end sequence of U6 small nuclear RNA. *Nature* **506**, 116–120 (2014).
49. Liu, S. *et al.* Binding of the human Prp31 Nop domain to a composite RNA-protein platform in U4 snRNP. *Science* **316**, 115–120 (2007).
50. Lin, P.-C. & Xu, R.-M. Structure and assembly of the SF3a splicing factor complex of U2 snRNP. *EMBO J.* **31**, 1579–1590 (2012).
51. Cretu, C. *et al.* Molecular architecture of SF3b and structural consequences of its cancer-related mutations. *Mol. Cell* **64**, 307–319 (2016).
52. Pomeranz Krummel, D.A., Oubridge, C., Leung, A.K.W., Li, J. & Nagai, K. Crystal structure of human spliceosomal U1 snRNP at 5.5-Å resolution. *Nature* **458**, 475–480 (2009).
53. Kondo, Y., Oubridge, C., van Roon, A.-M.M. & Nagai, K. Crystal structure of human U1 snRNP, a small nuclear ribonucleoprotein particle, reveals the mechanism of 5′ splice site recognition. *eLife* **4**, e04986 (2015).
54. Weber, G., Trowitzsch, S., Kastner, B., Lührmann, R. & Wahl, M.C. Functional organization of the Sm core in the crystal structure of human U1 snRNP. *EMBO J.* **29**, 4172–4184 (2010).
55. Stark, H. & Lührmann, R. Cryo-electron microscopy of spliceosomal components. *Annu. Rev. Biophys. Biomol. Struct.* **35**, 435–457 (2006).
56. Sander, B. *et al.* Organization of core spliceosomal components U5 snRNA loop I and U4–U6 di-snRNP within U4/U6–U5 tri-snRNP as revealed by electron cryomicroscopy. *Mol. Cell* **24**, 267–278 (2006).
57. Boehringer, D. *et al.* Three-dimensional structure of a pre-catalytic human spliceosomal complex B. *Nat. Struct. Mol. Biol.* **11**, 463–468 (2004).
58. Jurica, M.S., Sousa, D., Moore, M.J. & Grigorieff, N. Three-dimensional structure of C complex spliceosomes by electron microscopy. *Nat. Struct. Mol. Biol.* **11**, 265–269 (2004).
59. Golas, M.M. *et al.* 3D cryo-EM structure of an active step I spliceosome and localization of its catalytic core. *Mol. Cell* **40**, 927–938 (2010).
60. Ohi, M.D., Ren, L., Wall, J.S., Gould, K.L. & Walz, T. Structural characterization of the fission yeast U5–U2/U6 spliceosome complex. *Proc. Natl. Acad. Sci. USA* **104**, 3195–3200 (2007).
61. Cohen-Krausz, S., Sperling, R. & Sperling, J. Exploring the architecture of the intact supraspliceosome using electron microscopy. *J. Mol. Biol.* **368**, 319–327 (2007).
62. Kühlbrandt, W. Cryo-EM enters a new era. *eLife* **3**, e03678 (2014).
63. Fabrizio, P. *et al.* The evolutionarily conserved core design of the catalytic activation step of the yeast spliceosome. *Mol. Cell* **36**, 593–608 (2009).
64. Plaschka, C., Lin, P.-C. & Nagai, K. Structure of a pre-catalytic spliceosome. *Nature* **546**, 617–621 (2017).
This paper described the cryo-EM structure of the yeast spliceosomal B complex and provided insight into Brr2-mediated activation of the spliceosome.
65. Rauhut, R. *et al.* Molecular architecture of the *Saccharomyces cerevisiae* activated spliceosome. *Science* **353**, 1399–1405 (2016).
The structure of yeast spliceosome after Brr2-mediated activation, providing insight into Prp2-induced remodeling.
66. Yan, C., Wan, R., Bai, R., Huang, G. & Shi, Y. Structure of a yeast-activated spliceosome at 3.5-Å resolution. *Science* **353**, 904–911 (2016).
The 3.5-Å structure of the yeast B^{act} complex, which revealed that the active site is already formed but that the BP adenosine is kept 50 Å away from the active site by the U2 snRNP SF3b complex.
67. Nguyen, T.H. *et al.* The architecture of the spliceosomal U4/U6–U5 tri-snRNP. *Nature* **523**, 47–52 (2015)
The cryo-EM structure of the yeast U4/U6–U5 tri-snRNP that provided the first pseudo-atomic model of a spliceosomal complex, which revealed the organization of protein and RNA components.
68. Nguyen, T.H.D. *et al.* Cryo-EM structure of the yeast U4/U6–U5 tri-snRNP at 3.7-Å resolution. *Nature* **530**, 298–302 (2016).
This paper describes a complete atomic model of the 1.5-MDa U4/U6–U5 tri-snRNP and provides important new insights into the spliceosomal activation process that leads to the formation of the catalytic center.
69. Wan, R. *et al.* The 3.8-Å structure of the U4/U6–U5 tri-snRNP: insights into spliceosome assembly and catalysis. *Science* **351**, 466–475 (2016).
This paper also describes a complete atomic model of yeast U4/U6–U5 tri-snRNP and shows how U6 snRNA is kept catalytically inactive by the U4 snRNA and Prp3.
70. Wu, N.-Y., Chung, C.-S. & Cheng, S.-C. Role of Cwc24 in the first catalytic step of splicing and fidelity of 5′ splice site selection. *Mol. Cell. Biol.* **37**, e00580–e16 (2017).
71. Galej, W.P. *et al.* Cryo-EM structure of the spliceosome immediately after branching. *Nature* **537**, 197–201 (2016).
This study revealed the cryo-EM structure of a catalytic spliceosome with the products of the first catalytic reaction bound to the active site, elucidated how the BP adenosine docks into the active site for catalysis and provided structural insights into Prp16-dependent remodeling of the spliceosome for exon ligation.
72. Wan, R., Yan, C., Bai, R., Huang, G. & Shi, Y. Structure of a yeast catalytic step I spliceosome at 3.4-Å resolution. *Science* **353**, 895–904 (2016).
This paper also presented the cryo-EM structure of the catalytic spliceosome after the first step of splicing at 3.4-Å resolution, revealing the interactions between the substrates and surrounding proteins in detail.
73. Steitz, T.A. & Steitz, J.A. A general two-metal-ion mechanism for catalytic RNA. *Proc. Natl. Acad. Sci. USA* **90**, 6498–6502 (1993).
74. Yean, S.L., Wuenschell, G., Termini, J. & Lin, R.-J. Metal-ion coordination by U6 small nuclear RNA contributes to catalysis in the spliceosome. *Nature* **408**, 881–884 (2000).
75. Fica, S.M. *et al.* RNA catalyzes nuclear pre-mRNA splicing. *Nature* **503**, 229–234 (2013).
This study identified the U6 snRNA phosphate oxygens that coordinate catalytic metal ions for branching and exon ligations, demonstrating that both reactions are catalyzed by a single RNA-based active site.
76. Fica, S.M., Mefford, M.A., Piccirilli, J.A. & Staley, J.P. Evidence for a group II intron-like catalytic triplex in the spliceosome. *Nat. Struct. Mol. Biol.* **21**, 464–471 (2014).
77. Fica, S.M. *et al.* Structure of a spliceosome remodeled for exon ligation. *Nature* **542**, 377–380 (2017).
This paper presented the cryo-EM structure of a spliceosome just before the second catalytic step and showed how a Prp16-induced structural change undocks the branch helix from the active site and creates a space for the incoming 3′ exon for exon ligation.
78. Yan, C., Wan, R., Bai, R., Huang, G. & Shi, Y. Structure of a yeast step II catalytically activated spliceosome. *Science* **355**, 149–155 (2017).
This paper also describes the cryo-EM structure of the yeast C* spliceosome in atomic detail and provides functional insights similar to those in ref. 77.
79. Brys, A. & Schwer, B. Requirement for SLU7 in yeast pre-mRNA splicing is dictated by the distance between the branchpoint and the 3′ splice site. *RNA* **2**, 707–717 (1996).
80. Query, C.C. & Konarska, M.M. Suppression of multiple substrate mutations by spliceosomal *prp8* alleles suggests functional correlations with ribosomal ambiguity mutants. *Mol. Cell* **14**, 343–354 (2004).

81. Konarska, M.M., Vilardell, J. & Query, C.C. Repositioning of the reaction intermediate within the catalytic center of the spliceosome. *Mol. Cell* **21**, 543–553 (2006).
82. Liu, L., Query, C.C. & Konarska, M.M. Opposing classes of *prp8* alleles modulate the transition between the catalytic steps of pre-mRNA splicing. *Nat. Struct. Mol. Biol.* **14**, 519–526 (2007).
83. Query, C.C. & Konarska, M.M. *CEF1* (*CDC5*) alleles modulate transitions between catalytic conformations of the spliceosome. *RNA* **18**, 1001–1013 (2012).
84. Burgess, S.M. & Guthrie, C. A mechanism to enhance mRNA splicing fidelity: the RNA-dependent ATPase Prp16 governs usage of a discard pathway for aberrant lariat intermediates. *Cell* **73**, 1377–1391 (1993).
85. Mayas, R.M., Maita, H. & Staley, J.P. Exon ligation is proofread by the DExD/H-box ATPase Prp22p. *Nat. Struct. Mol. Biol.* **13**, 482–490 (2006).
86. Xu, Y.-Z. & Query, C.C. Competition between the ATPase Prp5 and branch region-U2 snRNA pairing modulates the fidelity of spliceosome assembly. *Mol. Cell* **28**, 838–849 (2007).
87. Lardelli, R.M., Thompson, J.X., Yates, J.R. III & Stevens, S.W. Release of SF3 from the intron branchpoint activates the first step of pre-mRNA splicing. *RNA* **16**, 516–528 (2010).
88. Wlodaver, A.M. & Staley, J.P. The DExD/H-box ATPase Prp2p destabilizes and proofreads the catalytic RNA core of the spliceosome. *RNA* **20**, 282–294 (2014).
89. Koodathingal, P., Novak, T., Piccirilli, J.A. & Staley, J.P. The DEAH-box ATPases Prp16 and Prp43 cooperate to proofread 5′ splice site cleavage during pre-mRNA splicing. *Mol. Cell* **39**, 385–395 (2010).
90. Reyes, J.L., Gustafson, E.H., Luo, H.R., Moore, M.J. & Konarska, M.M. The C-terminal region of hPrp8 interacts with the conserved GU dinucleotide at the 5′ splice site. *RNA* **5**, 167–179 (1999).
91. Siatecka, M., Reyes, J.L. & Konarska, M.M. Functional interactions of Prp8 with both splice sites at the spliceosomal catalytic center. *Genes Dev.* **13**, 1983–1993 (1999).
92. Collins, C.A. & Guthrie, C. Allele-specific genetic interactions between Prp8 and RNA active site residues suggest a function for Prp8 at the catalytic core of the spliceosome. *Genes Dev.* **13**, 1970–1982 (1999).
93. Yan, C. *et al.* Structure of a yeast spliceosome at 3.6-Å resolution. *Science* **349**, 1182–1191 (2015).
The cryo-EM structure of the *S. pombe* intron-lariat spliceosome revealed the structure of the active site after mRNA release and provided a first view of the active site and the Prp19-associated complex.
94. Garrey, S.M. *et al.* A homolog of lariat-debranching enzyme modulates turnover of branched RNA. *RNA* **20**, 1337–1348 (2014).
95. Bertram, K. *et al.* Cryo-EM structure of a human spliceosome activated for step 2 of splicing. *Nature* **542**, 318–323 (2017).
The structure of a human C* spliceosome is remarkably similar to its yeast counterpart, but notably two yeast proteins, Cwc2 and Ecm2, were fused to one polypeptide.
96. Zhang, X. *et al.* An atomic structure of the human spliceosome. *Cell* **169**, 918–929.e14 (2017).
This paper presented a high-resolution structure of a human spliceosome and uncovered mammal-specific protein factors that stabilized the human C* conformation.
97. De, I. *et al.* The RNA helicase Aquarius exhibits structural adaptations mediating its recruitment to spliceosomes. *Nat. Struct. Mol. Biol.* **22**, 138–144 (2015).
98. Agafonov, D.E. *et al.* Molecular architecture of the human U4/U6–U5 tri-snRNP. *Science* **351**, 1416–1420 (2016).
The 7-Å cryo-EM structure of the human tri-snRNP shows that SAD1 tethers the BRR2 helicase at the pre-activation position and keeps it away from the substrate U4 snRNA.
99. Wolf, E. *et al.* Exon, intron and splice site locations in the spliceosomal B complex. *EMBO J.* **28**, 2283–2292 (2009).
100. Bertram, K. *et al.* Cryo-EM structure of a pre-catalytic human spliceosome primed for activation. *Cell* **170**, 701–713.e11 (2017).
This study presents the structure of a human B complex, revealing how the BRR2 helicase binds the U4 snRNA substrate at the same position as in the yeast B complex.